Available online at www.sciencedirect.com
ScienceDirect
Trans. Nonferrous Met. Soc. China 28(2018) 957−965
Transactions of Nonferrous Metals Society of China
www.tnmsc.cn

Microstructure, sintering behavior and mechanical properties of $SiC/MoSi_2$ composites by spark plasma sintering

Xin-xin HAN, Ya-lei WANG, Xiang XIONG, Heng LI, Zhao-ke CHEN, Wei SUN

State Key Laboratory of Powder Metallurgy, Central South University, Changsha 410083, China

Received 26 December 2016; accepted 22 June 2017

Abstract: $SiC/MoSi_2$ composites were synthesized at different temperatures by spark plasma sintering using Mo, Si and SiC powders as raw materials. The phase composition, microstructure and mechanical properties of the as-prepared composites were investigated and the sintering behavior was also discussed. Results show that $SiC/MoSi_2$ composites are composed of $MoSi_2$, SiC and trace amount of $Mo_{4.8}Si_3C_{0.6}$ phase and exhibit a fine-grain texture. During the synthesis process, there was an evolution from solid phase sintering to liquid phase sintering. When sintered at 1600 °C, the $SiC/MoSi_2$ composites present the most favorable mechanical properties, the Vickers hardness, bending strength and fracture toughness are 13.4 GPa, 674 MPa and 5.1 $MPa·m^{1/2}$, respectively, higher 44%, 171%, 82% than those of monolithic $MoSi_2$. SiC can withstand the applied stress as hard phase and retard the rapid propagation of cracks as second phase, which are beneficial to the improved mechanical properties of $SiC/MoSi_2$ composites.
Key words: $SiC/MoSi_2$ composite; microstructure; sintering behavior; mechanical properties; spark plasma sintering

1 Introduction

Molybdenum disilicide ($MoSi_2$) is considered as a promising structural material for high temperature applications due to its medium density (6.24 g/cm^3), high melting point (2030 °C), favorable high-temperature oxidation resistance, good electrical conductivity and thermal conductivity [1,2]. However, monolithic $MoSi_2$ exhibits poor ductility at room temperature and low creep resistance at elevated temperature, which limits the practical applications of $MoSi_2$ [3]. Therefore, it is essential to improve the ambient toughness and high-temperature strength of monolithic $MoSi_2$. Researches have shown that the mechanical properties of $MoSi_2$ can be improved significantly by means of adding second phase reinforcements in form of particles or whiskers, such as SiC, Si_3N_4, TiC, Al_2O_3, La_2O_3 [4−9]. Among them, SiC has favorable high-temperature strength and oxidation resistance, matched elastic modulus as well as excellent thermodynamic stability and wettability to $MoSi_2$, which results in SiC as ideal modified component in improving the mechanical properties of $MoSi_2$ [10].

SiC modified $MoSi_2$ matrix ($SiC/MoSi_2$) composites can be prepared by hot pressing [4], self-propagating high temperature synthesis [11], microwave sintering [12], pressureless sintering [13] and spark plasma sintering (SPS) [14,15]. For instance, PANNEERSELVAM et al [12] synthesized $SiC/MoSi_2$ composites with commercial SiC and $MoSi_2$ powders by microwave sintering, the results show that as the SiC content changes, the fracture toughness of the composites can reach a peak value of 4.5 $MPa·m^{1/2}$ with 20% SiC (volume fraction) addition. CHEN et al [16] prepared 20%$SiC/MoSi_2$ composites using Mo, Si and C element powders, the bending strength, Vichers hardness and fracture toughness of the composites can reach 324.6 MPa, 10.3 GPa and 6.32 $MPa·m^{1/2}$, respectively，which are also higher than those of traditional $MoSi_2$. In addition, ESMAEILY et al [14] prepared $SiC/MoSi_2$ composites by SPS using Mo, Si and C element powders, the mechanical properties were also enhanced greatly with the addition of SiC second phase. As an innovative rapid-sintering technology with advantages of lower sintering temperature, short sintering time and simple operation, SPS has been widely applied to preparing functional graded materials [17], hard alloys [18], ceramic materials [19] and metal matrix composites [20], and so on. Meanwhile, the prepared materials are easily

Foundation item: Project (2014M562129) supported by the Postdoctoral Fund Project of China
Corresponding author: Ya-lei WANG; Tel: +86-731-88876134; E-mail: yaleipm@csu.edu.cn
DOI: 10.1016/S1003-6326(18)64730-2

to obtain fine-grain texture and high density [21], which is beneficial to the mechanical performances of $SiC/MoSi_2$ composites. However, there are limited studies reported thus far on the microstructure, sintering behavior and mechanical properties of $SiC/MoSi_2$ composites synthesized by SPS using Mo, Si and SiC powders.

In present work, $SiC/MoSi_2$ composites were synthesized by SPS using Mo, Si and SiC powders at different temperatures. The phase composition, microstructure and mechanical properties of $SiC/MoSi_2$ composites were investigated. The sintering behavior was also discussed in detail. The work can provide data and theoretical basis for further research and application of $MoSi_2$ matrix composites.

2 Experimental

99.95% pure Mo powder with an average size of 2 μm, 99.99% pure Si powder with an average size of 10 μm and 99.9% pure SiC powder with an average size of 500 nm were used as raw materials in present study. The above powder materials were mixed corresponding to composition of 20% SiC and 80% $MoSi_2$. The powder mixture was then ball-milled for 8 h by ZrO_2 balls under argon with alcohol as milling media. The ball to powder ratio was 3:1 and the rotation speed was 225 r/min. After ball-milling, the resultant slurry was dried at 60 °C for 12 h in a vacuum drying oven for removing alcohol. Finally, the dried powder mixture was ground and passed through a 300-mesh sieve.

The prepared powder mixture was firstly loaded into a cylindrical carbon/carbon (C/C) composite die (d60 mm × 30 mm × 48 mm) lined with graphite foil, and then the powder-loaded die was placed into the SPS reaction chamber. At last, $SiC/MoSi_2$ composites were synthesized by spark plasma sintering at different temperatures. In addition, monolithic $MoSi_2$ was also synthesized by SPS using Mo and Si powders. The detailed sintering parameters of SPS for $SiC/MoSi_2$ composites (MSSC) and monolithic $MoSi_2$ (MS) are listed in Table 1.

The bulk densities of the synthesized samples were evaluated by Archimedes method. The phase composition was investigated by D/max 2550VB+18 kW rotating target X-ray diffraction (XRD) (Rigaku Ltd., Japan, Cu K_α radiation). Microstructure and fracture morphology of the as-prepared samples were characterized by scanning electron microscopy (SEM, FEI NOVA Nano 230). The element composition and distribution were analyzed by electron microprobe (EPMA) equipped with wavelength dispersive X-ray spectrometer (WDS). The prepared samples were machined into 26 mm × 4 mm × 3 mm bars for mechanical test. The flexural strength (σ_b) was measured at room temperature using three-point bending test with a span length of 20 mm and loading rate of 0.5 mm/min. At least 5 bars for each specimen were tested for obtaining the corresponding flexural strength data. The Vickers hardness (HV) and fracture toughness (K_{IC}) for each sample were measured using HVS−5 Vickers hardness tester with a load of 5 kg for 10 s. The K_{IC} values were calculated using the equation reported by ANSTIS et al [22]. At least 10 points were measured on each sample.

3 Results and discussion

3.1 Phase identification

Figure 1 shows the XRD patterns of $SiC/MoSi_2$ composites prepared by SPS at different temperatures and the XRD pattern of monolithic $MoSi_2$ is also shown. It can be seen that there is no obvious difference in phase composition for all prepared $SiC/MoSi_2$ composites. The as-prepared composites are mainly composed of $MoSi_2$ and SiC phases. $MoSi_2$ is the major phase and SiC is the second phase. Meanwhile, trace amount of $Mo_{4.8}Si_3C_{0.6}$ (Nowotny phase) can also be detected, which can also play a role as a reinforcement phase for $SiC/MoSi_2$ composites [23,24]. For monolithic $MoSi_2$, XRD analysis indicates that it consists of $MoSi_2$ and tiny amount of Mo_5Si_3, and the formation of Mo_5Si_3 can be attributed to the silicon loss during the SPS sintering process.

It is worth noticing that $Mo_{4.8}Si_3C_{0.6}$ phase was formed in $SiC/MoSi_2$ composites, which is different from the Mo_5Si_3 phase formed in monolithic $MoSi_2$. For revealing the reaction process of Mo−Si−SiC system as well as the phase evolution during SPS, the prepared

Table 1 Sintering parameters of SPS for $SiC/MoSi_2$ and $MoSi_2$

Sample	Sintering temperature/°C	Heating rate/ (°C·min^{-1})	Cooling rate/ (°C·min^{-1})	Holding time/min	Pressure/ MPa
MSSC13	1300	100	100	10	40
MSSC14	1400	100	100	10	40
MSSC15	1500	100	100	10	40
MSSC16	1600	100	100	10	40
MS	1300	100	100	5	40

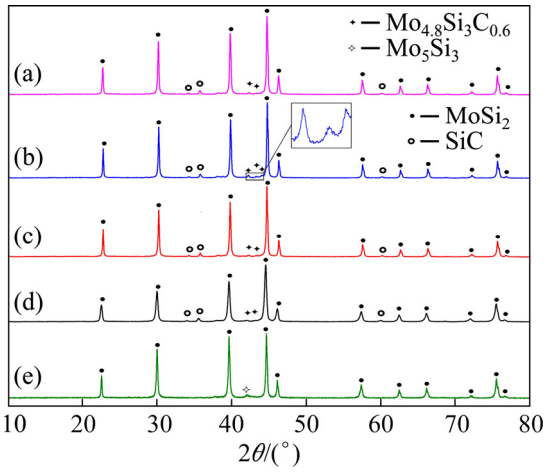

Fig. 1 XRD patterns of SiC/$MoSi_2$ composites and monolithic $MoSi_2$ prepared by SPS: (a) MSSC13; (b) MSSC14; (c) MSSC15; (d) MSSC16; (e) MS

powder mixture was also sintered by SPS at 850, 1050, 1150 and 1200 °C, respectively. Figure 2 shows the XRD patterns of the products sintered at low temperatures. It can be seen that only the characteristic peaks of Mo, Si and SiC are observed in the XRD pattern (Fig. 2(a)), which indicates that the treatment temperature (850 °C) is not high enough to trigger the chemical reactions in Mo−Si−SiC system. When sinterd at 1050 °C, as shown in Fig. 2(b), besides Mo, Si and SiC diffraction peaks, minor Mo_3Si, Mo_2C and Mo_5Si_3 peaks began to appear in the pattern. Mo_3Si and Mo_5Si_3 phases were formed mainly due to the reaction between Mo and Si powders, and the formation of Mo_2C should be related to the chemical reaction between SiC and Mo [10]. With the sintering temperature increasing to 1150 °C, $MoSi_2$ peaks can be observed in the XRD pattern (Fig. 2(c)), indicating the formation of $MoSi_2$ phase. The weak peaks of $MoSi_2$ represent the insufficient reactions in Mo−Si−SiC system at 1150 °C. As shown in Fig. 2(d), it

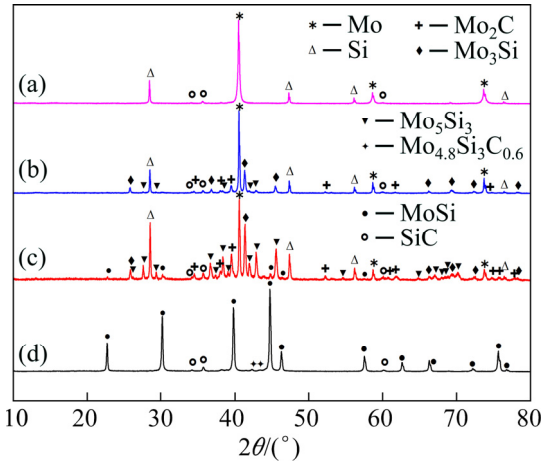

Fig. 2 XRD patterns of products sintered at low temperatures: (a) 850 °C; (b) 1050 °C; (c) 1150 °C; (d) 1200 °C

is obvious that all of the Mo, Si characteristic peaks disappeared after sintering at 1200 °C. The synthesized product was composed of $MoSi_2$, SiC and minor $Mo_{4.8}Si_3C_{0.6}$, which indicates the complete reactions of Mo−Si−SiC system as well as the synthesis of SiC/$MoSi_2$ composites. Therefore, it can be inferred that the $MoSi_2$ phase was mainly formed due to the reactions between Mo or Mo-riched phases and Si and the formation of $Mo_{4.8}Si_3C_{0.6}$ phase may be related to the reaction between Mo_2C and Si. Moreover, the reaction rate of Mo−Si−SiC system accelerated significantly due to the improved diffusion rate of reactants at increased sintering temperature.

3.2 Microstructure of SiC/$MoSi_2$ composites

Figure 3 shows the structural backscattered electron (BSE) images of SiC/$MoSi_2$ composites sintered at various temperatures. It can be seen that three kinds of phases (gray, dark and light phases) can be observed in all the as-prepared SiC/$MoSi_2$ composites. For identifying the element compositions of these various phases, the as-prepared SiC/$MoSi_2$ composites were analyzed by EPMA equipped with wavelength dispersive X-ray spectrometer (WDS). Figure 4 shows the enlarged structural BSE image of SiC/$MoSi_2$ composite (MSSC16) as well as the element distribution maps of Mo, Si and C. It can be seen that the Mo element is mainly distributed in gray and light phases (Fig. 4(b)), the Si element is mainly assembled in dark and gray phases (Fig. 4(c)). Moreover, C element mainly exists in dark phase (Fig. 4(d)). Table 2 lists the mole fractions of Mo, Si and C in different phases. Combined with the analysis of element distribution maps (Fig. 4) and the XRD patterns (Fig. 1), it can be deduced that the gray, dark and light phases are corresponding to $MoSi_2$, SiC and $Mo_{4.8}Si_3C_{0.6}$, respectively. In SiC/$MoSi_2$ composites, the SiC particles are mainly distributed at the boundaries among the adjacent $MoSi_2$ grains, which could play a role in pinning the grain boundaries and then inhibit the grain growth of $MoSi_2$ during the sintering process. Meanwhile, tiny amount of SiC phase was embedded in the $MoSi_2$ crystals and resulted in an intragranular structure, which can also refine the grains of $MoSi_2$ due to the generation of secondary interface. Moreover, the SiC phase exhibits a poor homogeneity distribution in SiC/$MoSi_2$ composites sintered at lower temperatures (1300 and 1400 °C). However, when sintered at higher sintering temperatures (1500 and 1600 °C), the SiC phase presents a more uniform distribution in SiC/$MoSi_2$ composites compared with the SiC/$MoSi_2$ composites prepared by SPS using Mo, Si and C powders [14,25].

Figure 5 shows the SEM images of SiC/$MoSi_2$ composites sintered at different temperatures. It can be seen that the SiC/$MoSi_2$ composites exhibit a difference

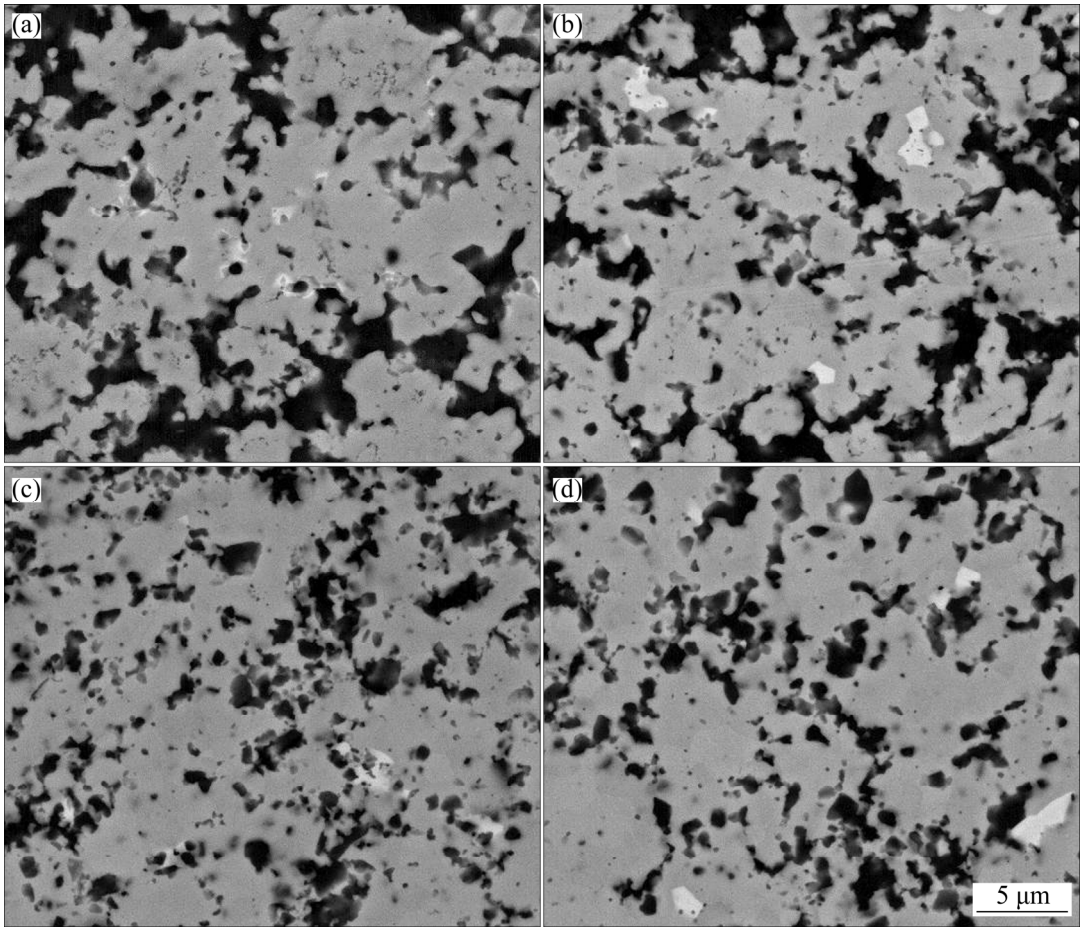

Fig. 3 Structural backscattered electron images of SiC/$MoSi_2$ composites: (a) MSSC13; (b) MSSC14; (c) MSSC15; (d) MSSC16

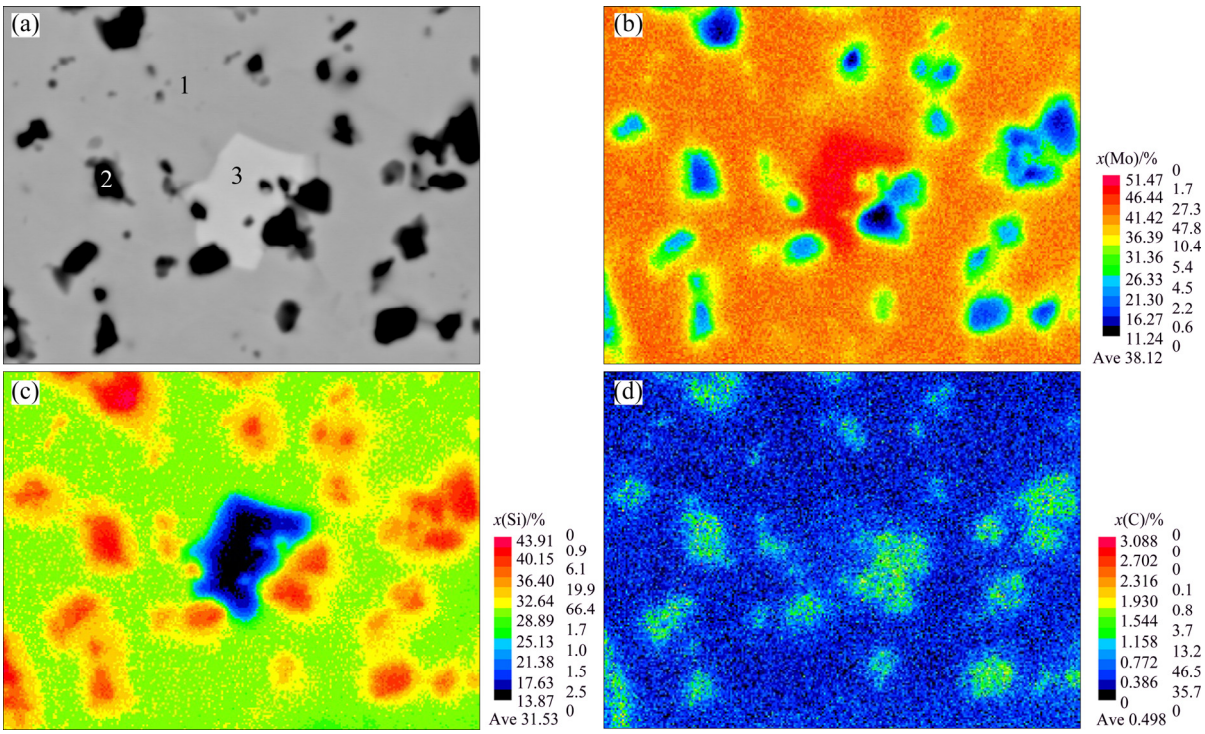

Fig. 4 Enlarged structural BSE image (a) of MSSC16 and elemental distributions of Mo (b), Si (c) and C (d)

Table 2 Mole fraction of Mo, Si and C obtained from $SiC/MoSi_2$ composites

Point in Fig. 4(a)	Mole fraction/%			Molecular formula
	Mo	Si	C	
Point 1	33.04	66.96	−	$MoSi_2$
Point 2	−	51.89	48.11	SiC
Point 3	59.30	34.30	6.40	$Mo_{4.8}Si_3C_{0.6}$

in microstructure, the densification of $SiC/MoSi_2$ composites was significantly enhanced with the elevated sintering temperature. When sintered at 1300 and 1400 °C, a large amount of connected pores can be observed in the composites (Figs. 5(a) and (b)). With the sintering temperature increasing to 1500 °C, the $SiC/MoSi_2$ composites exhibit denser structure than that sintered at 1300 and 1400 °C (Fig. 5(c)). Only spherical pores can be found in the composite organization, the quantity and size of pores are also lower than that sintered at 1300 and 1400 °C. After being sintered at 1600 °C, as shown in Fig. 5(d), it can be seen that there are no obvious pores in $SiC/MoSi_2$ composites, indicating the high densification of the $SiC/MoSi_2$ composites. In addition, the $SiC/MoSi_2$ composites can achieve favorable densification without exaggerated grain growth during the sintering process (Fig. 5(d)).

3.3 Sintering behavior of $SiC/MoSi_2$ composites

During the SPS sintering process of $SiC/MoSi_2$ composites, there was an obvious exothermic phenomenon accompanied with a sharp increase in displacement at 1184 °C, which indicates that chemical reactions in Mo−Si−SiC system take place violently at this moment. In addition, it can be seen from Fig. 2 that the phase composition had a substantial transformation with the sintering temperature changing from 1150 to 1200 °C, which may be attributed to the appearance of liquid silicon ($T_{m(Si)}$=1410 °C). Indeed the temperature field has a non-uniform distribution in the sintered body in the SPS equipment. The monitored temperature near the edge of the die is usually far lower than that at the center of the sintered sample [26,27], which is responsible for the appearance of liquid silicon between 1150 and 1200 °C in present study. Based on the phase evolution of the sintered products at low temperatures (Fig. 2) as well as the structural characters of $SiC/MoSi_2$ composites, a sintering model was proposed in this study. Figure 6 shows the schematic diagrams of sintering process for $SiC/MoSi_2$ composites synthesized by SPS. As shown in Fig. 6(a), the powder mixture was just compacted at low temperature, no any reaction happened in this stage. With the temperature increasing, Mo_3Si, Mo_5Si_3 and Mo_2C intermediate phases generated firstly

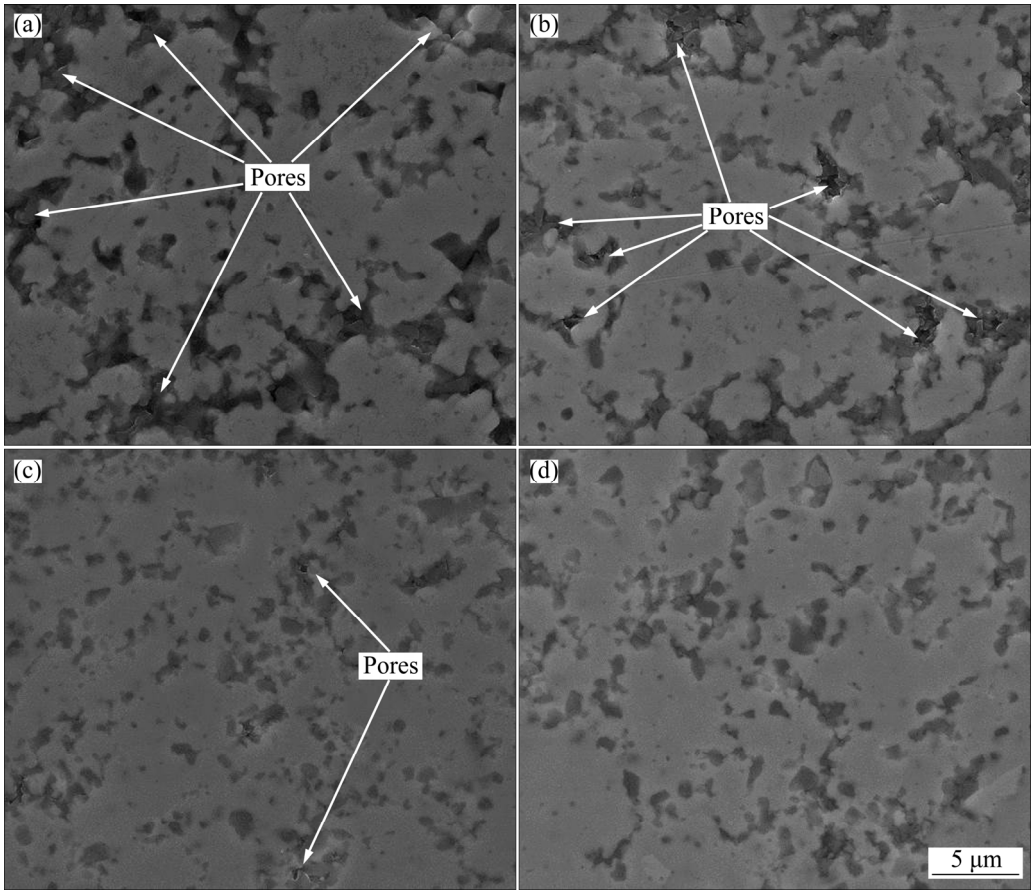

Fig. 5 SEM images of $SiC/MoSi_2$ composites: (a) MSSC13; (b) MSSC14; (c) MSSC15; (d) MSSC16

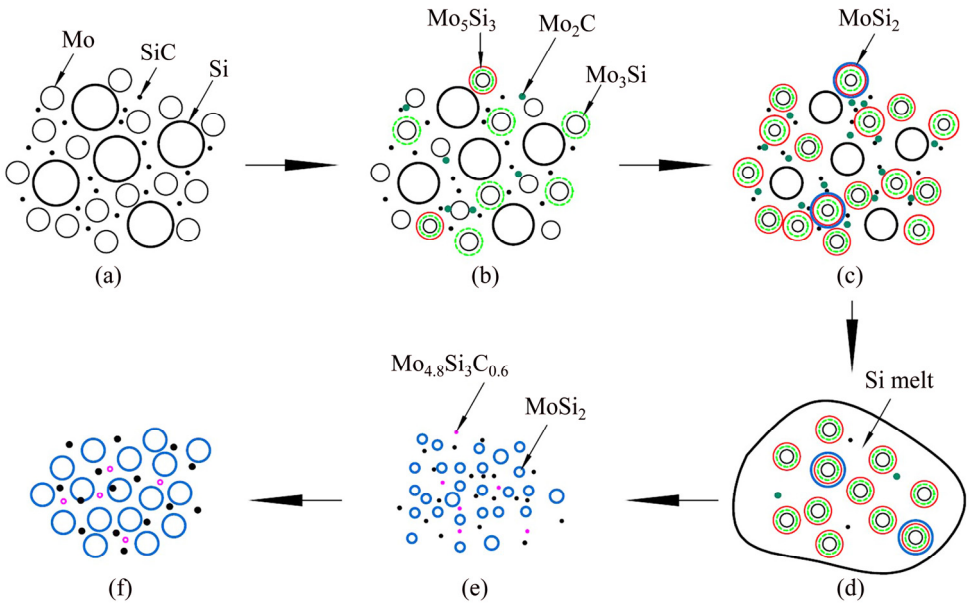

Fig. 6 Schematic diagrams of sintering process for SiC/$MoSi_2$ composites synthesized by SPS

in Mo−Si−SiC system. In this stage, a Mo−Si compound layer was formed on the surface of Mo particles through solid−solid reaction (Fig. 6(b)), which can be represented as: Mo+Si→Mo_3Si+Si→Mo_5Si_3 [28]. Meanwhile, the residual Si diffused through the compound layer and then reacted with Mo to form Mo−Si compounds continuously [28], no $MoSi_2$ phase was formed due to the lower diffusion rate of Si at low temperature. XRD results can also prove that the Mo-rich intermediate phases were formed prior to $MoSi_2$ phase (Fig. 2). In addition, Mo_2C phase was also formed due to the reaction between Mo and SiC in this stage [10]. With the temperature increasing gradually, $MoSi_2$ phase generated continuously due to the accelerated diffusion rate of Si (Fig. 6(c)). When the temperature reached a certain value, $MoSi_2$ phase was formed instantaneously accompanied with the rapid densification of SiC/$MoSi_2$ composites, which is attributed to the appearance of liquid silicon (Fig. 6(d)). It is reported that the mobility of liquid silicon is 10^3~10^5 times that of solid silicon [29], which is responsible for the rapid formation of $MoSi_2$. With the appearance of liquid silicon, the liquid silicon can wet SiC, Mo and other intermediate solid phases, a kind of strong capillary tension developed, which can lead to the particles rearrangement and pores shrinkage [14]. Meanwhile, certain small solid particles can dissolve into liquid Si, α-$MoSi_2$ was precipitated from supersaturated liquid Si. Moreover, the $Mo_{4.8}Si_3C_{0.6}$ phase was also formed in the composites (Fig. 6(e)). Therefore, it can be inferred that the sintering process of SiC/$MoSi_2$ composites experienced a transformation from solid phase sintering to liquid phase sintering. The inhibition effect of SiC phase on the growth of $MoSi_2$ grains can induce the formation of fine organization structure for SiC/$MoSi_2$ composites (Fig. 6(f)).

3.4 Mechanical properties of SiC/$MoSi_2$ composites

Table 3 shows the relative densities and mechanical properties of SiC/$MoSi_2$ composites synthesized at different temperatures. The theoretical density of 20%SiC/$MoSi_2$ composites (5.632 g/cm^3) was obtained by the additivity rule of composite materials. It can be seen from Table 3 that the densities of SiC/$MoSi_2$ composites are all greater than 90% of the theoretical density and present a upward tendency with the increased sintering temperature. Although the SiC/$MoSi_2$ composites can achieve relatively high densities, they are still smaller than that of monolithic $MoSi_2$ (99.3%) sintered at 1300 °C, which should be related to the higher sintering temperature of SiC phase [30]. In addition, the mechanical property of SiC/$MoSi_2$ composites is significantly higher than that of monolithic $MoSi_2$, indicating that the addition of SiC phase can effectively improve the mechanical properties of $MoSi_2$. The lower Vickers hardness of MSSC13 compared with that of monolithic $MoSi_2$ is mainly attributed to the higher porosity of the SiC/$MoSi_2$ composites. Moreover, the mechanical properties of SiC/$MoSi_2$ composites increase gradually with the elevated temperature in the range of temperature investigated in present study. When being sintered at 1600 °C, the SiC/$MoSi_2$ composite has the most favorable mechanical properties: the Vickers hardness (HV), bending strength (σ_b) and fracture toughness (K_{IC}) are 13.4 GPa, 674 MPa and

5.1 MPa·m$^{1/2}$, respectively, which are higher 44%, 171%, 82% than those of monolithic $MoSi_2$.

Table 3 Relative densities and mechanical properties of $SiC/MoSi_2$ composites

Sample	Relative density/%	HV/ GPa	σ_b/ MPa	K_{IC}/ (MPa·m$^{1/2}$)
MSSC13	90.2±0.3	7.2±0.3	432±13	3.3±0.2
MSSC14	91.8±0.2	9.6±0.4	585±32	3.8±0.3
MSSC15	96.8±0.2	12.6±0.3	640±12	4.0±0.2
MSSC16	97.8±0.1	13.4±0.3	674±38	5.1±0.4
MS	99.3±0.3	9.3±0.2	249±15	2.8±0.3

Figure 7 shows the fracture morphologies of monolithic $MoSi_2$ and $SiC/MoSi_2$ composites. It can be seen from Fig. 7(a) that the monolithic $MoSi_2$ has a smooth fracture with obvious river patterns and cleavage steps, exhibiting a typical transgranular fracture behavior. Figures 7(b) and (c) present the fracture morphologies of $SiC/MoSi_2$ composites sintered at 1300 and 1600 °C. It can be seen that the grain size of $MoSi_2$ phase in $SiC/MoSi_2$ composites is far smaller than that in monolithic $MoSi_2$, which indicates that SiC phase can effectively prevent the $MoSi_2$ grain growth during sintering process, and then result in fine organization for $SiC/MoSi_2$ composites. The formation of fine organization structure can release the thermal stress in composites generated during the cooling process, as a result, a strong-bonded interface can be formed between $MoSi_2$ and SiC. Moreover, with the introduction of SiC phase in $MoSi_2$ matrix, the fracture surface exihibits a mixed feature with much intergranular fracture. Owing to the fine orgnazition and intergranular fracture, the crack propagates more circuitously and consumes more fracture energy, which results in the improvement in mechanical properties of $SiC/MoSi_2$ composites.

Figure 8 shows the crack propagation path in monolithic $MoSi_2$ and $SiC/MoSi_2$ composites generated by room temperature hardness indent. It can be seen that the crack propagates in straight way in monolithic $MoSi_2$. Meanwhile, a zigzag crack with some branching can be observed in $SiC/MoSi_2$ composites resulted from the traction force of SiC phase. As the crack advances, the crack driving force can be rapidly exhausted due to crack deflection and branching, which results in the termination and disappearance of the crack. Therefore, the SiC can withstand the applied stress as hard phase and retard the rapid propagation of cracks as second phase, which are beneficial to the improved mechanical properties of $SiC/MoSi_2$ composites.

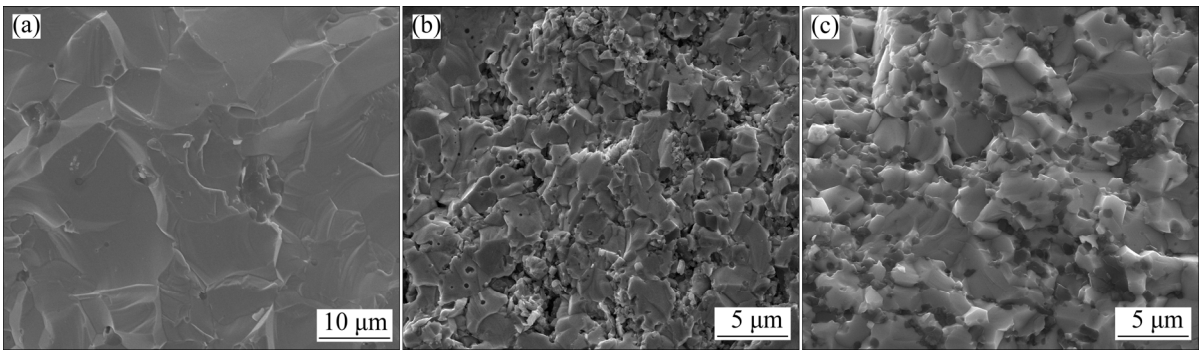

Fig. 7 Fracture morphologies of monolithic $MoSi_2$ as well as $SiC/MoSi_2$ composites: (a) MS; (b) MSSC13; (c) MSSC16

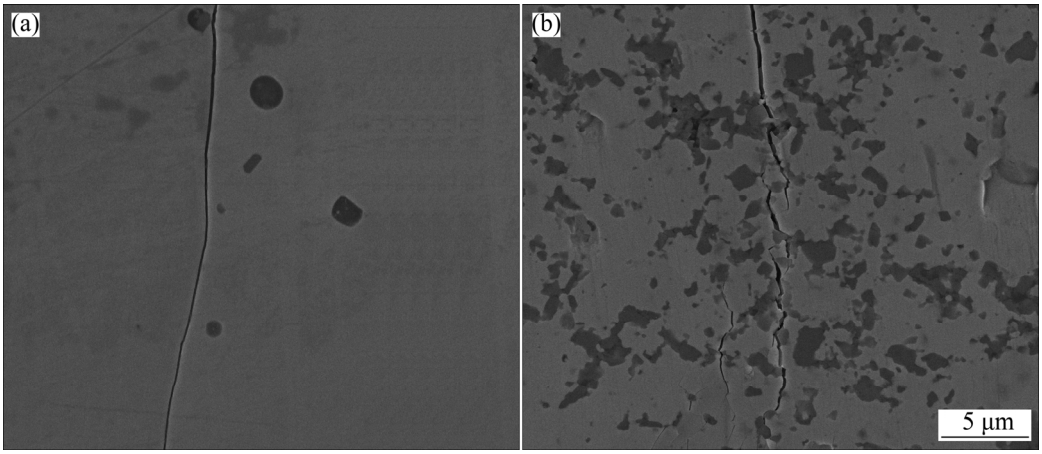

Fig. 8 SEM micrographs of crack propagation in $MoSi_2$ (a) and $SiC/MoSi_2$ composites (b)

4 Conclusions

1) The as-prepared SiC/$MoSi_2$ composites are composed of $MoSi_2$, SiC and trace amount of $Mo_{4.8}Si_3C_{0.6}$ phases in the sintering temperature range of 1300−1600 °C.

2) There is an evolution from solid phase sintering to liquid phase sintering during the synthesis process of SiC/$MoSi_2$ composites.

3) A fine-grain organization can be formed for SiC/$MoSi_2$ composites due to the introduction of SiC phase. The SiC phase can withstand the applied stress and trigger the formation of micro-cracks as well as retard the rapid propagation of cracks, which are responsible for the enhancement of mechanical properties for SiC/$MoSi_2$ composites.

4) The density and mechanical properties of SiC/$MoSi_2$ composites increase gradually with the elevated sintering temperature. The SiC/$MoSi_2$ composites have the most favorable mechanical properties with the sintering temperature 1600 °C, the Vickers hardness, bending strength and fracture toughness are 13.4 GPa, 674 MPa and 5.1 MPa·$m^{1/2}$, respectively, which are higher 44%, 171%, 82% than those of monolithic $MoSi_2$.

References

[1] AIKIN R M. On the ductile-to-brittle transition temperature in $MoSi_2$ [J]. Scripta Metallurgica et Materialia, 1992, 26: 1025−1030.

[2] VASUDEVAN A K, PETROVIC J J. A comparative overview of molybdenum disilicide composites [J]. Materials Science and Engineering A, 1992, 115(1−2): 1−17.

[3] COSTA E SILVA A, KAUFMAN M J. Applications of in situ reactions to $MoSi_2$-based materials [J]. Materials Science and Engineering A, 1995, 195: 75−88.

[4] WANG Zhi, LI Shi-chao, WANG Min, WU Guo-qiang, SUN Xi-miao, LIU Min-jing. Effect of SiC whiskers on microstructure and mechanical properties of the $MoSi_2$−SiC_W composites [J]. International Journal of Refractory Metals and Hard Materials, 2013, 41(4): 489−494.

[5] HE Zi-bo, LI He-jun, SHI Xiao-hong, FU Qian-gang, WU Heng. Formation mechanism and oxidation behavior of $MoSi_2$−SiC protective coating prepared by chemical vapor infiltration/reaction [J]. Transactions of Nonferrous Metals Society of China, 2013, 23(7): 2100−2106.

[6] KO I Y, KANG H S, DOH J M, YOON J K, SHON I J. Properties and densification of nanocrystalline $MoSi_2$−Si_3N_4 composite from mechanically alloyed powders by pulsed current-activated sintering [J]. Journal of Alloys and Compounds, 2010, 502(1): L10−L13.

[7] YAN Jian-hui, ZHANG Hou-an, LI Yi-min. Mechanical properties and oxidation resistance behavior of TiC−TiB_2 reinforced $MoSi_2$ composites [J]. Transactions of Nonferrous Metals Society of China, 2009, 19(8): 1424−1430.

[8] HUANG Zhi-bin, ZHOU Wan-cheng, TANG Xiu-feng, ZHU Jian-kun. Effects of milling methods on the dielectric and the mechanical properties of hot-pressed sintered $MoSi_2$/Al_2O_3 composites [J]. Journal of Alloys and Compounds, 2011, 509(5): 1920−1923.

[9] GAO Jian-ying, JIANG Wan. Effect of La_2O_3 addition to modification of grain-boundary phase in $MoSi_2$ [J]. Journal of Alloys and Compounds, 2009, 476(1−2): 667−670.

[10] WEI Wen-cheng, LEE J S. Formation and reaction kinetics of Mo and Mo silicides in the preparation of $MoSi_2$/SiC composites [J]. Journal of the European Ceramic Society, 1998, 18(5): 509−520.

[11] XU Jian-guang, ZHANG Bao-lin, JIANG Guo-jian, LI Wen-lan, ZHUANG Han-rui. Synthesis of SiC_W/$MoSi_2$ powder by the "chemical oven" self-propagating combustion method [J]. Ceramics International, 2006, 32(6): 633−636.

[12] PANNEERSELVAM M, AGRAWAL A, RAO K J. Microwave sintering of $MoSi_2$−SiC composites [J]. Materials Science and Engineering A, 2003, 356(3): 267−273.

[13] CHEN Fang, XU Jian-guang, HOU Zhou-fu. In situ pressureless sintering of SiC/$MoSi_2$ composites [J]. Ceramics International, 2012, 38(4): 2767−2772.

[14] ESMAEILY S, KERMANI M, RAZAVI M, RAHIMIPOUR M R, ZAKERI M. An investigation on the in situ synthesis−sintering and mechanical properties of $MoSi_2$−xSiC composites prepared by spark plasma sintering [J]. International Journal of Refractory Metals and Hard Materials, 2015, 48: 263−271.

[15] XU Jian-guang, ZHANG Hou-an, JIANG Guo-jian, ZHANG Bao-lin, LI Wen-lan. SiC whisker reinforced $MoSi_2$ composite prepared by spark plasma sintering from COSHS-ed powder [J]. Transactions of Nonferrous Metals Society of China, 2006, 16(s2): s504−s507.

[16] CHEN Fang, XU Jian-guang, YAN Jian-hui, TANG Si-wen. Effects of Y_2O_3 on SiC/$MoSi_2$ composite by mechanical-assistant combustion synthesis [J]. International Journal of Refractory Metals and Hard Materials, 2013, 36(1): 143−148.

[17] MORIN C, LE GALLET S, ARIANE M, BERNARD F. Spark plasma sintering tool design for preparing alumina-based functionally graded materials [J]. Ceramics International, 2016, 42(2): 3056−3063.

[18] SIWAK P, GARBIEC D. Microstructure and mechanical properties of WC−Co, WC−Co−Cr_3C_2 and WC−Co−TaC cermets fabricated by spark plasma sintering [J]. Transactions of Nonferrous Metals Society of China, 2016, 26(10): 2641−2646.

[19] DEMIRSKYI D, VASYLKIV O. Hot-spots generation, exaggerated grain growth and mechanical performance of silicon carbide bulks consolidated by flash spark plasma sintering [J]. Journal of Alloys and Compounds, 2017, 691: 466−473.

[20] ZHANG Zhao-hui, SHEN Xiang-bo, WANG Fu-chi, WEI Sai, LI Shu-kui, CAI Hong-nian. Microstructure characteristics and mechanical properties of TiB/Ti−1.5Fe−2.25Mo composites synthesized in situ using SPS process [J]. Transactions of Nonferrous Metals Society of China, 2013, 23(9): 2598−2604.

[21] AVAREZ I, TORRECILLAS R, SOLIS W, PERETYAGIN P, FERNANDEZ A. Microstructural design of Al_2O_3−SiC nanocomposites by spark plasma sintering [J]. Ceramics International, 2016, 42(15): 17248−17253.

[22] ANSTIS G R, CHANTIKUL P, LAWN B R, MARSHALL D B. A critical evaluation of indentation techniques for measuring fracture toughness: I. Direct crack measurements [J]. Journal of the American Ceramic Society, 1981, 64(9): 533−538.

[23] MALOY S, HEUER A H, LEWANDOWSKI J, PETROVIC J. Carbon additions to molybdenum disilicide: Improved high-temperature mechanical properties [J]. Journal of the American Ceramic Society, 1991, 74(10): 2704−2706.

[24] SUZUKI Y, NIIHARA K. Synthesis and mechanical properties of $Mo_{\leq 5}Si_3C_{\leq 1}$ and $Mo_{\leq 5}Si_3C_{\leq 1}$-based composites [J]. Intermetallics, 1998, 6(1): 7−13.

[25] HU Qiao-dan, LUO Peng, YAN You-wei. Microstructures and densification of $MoSi_2$−SiC composite by field-activated and pressure-assisted combustion synthesis [J]. Journal of Alloys and Compounds, 2009, 468(1−2): 136−142.

[26] WANG Yu-cheng, FU Zheng-yi. Study of temperature field in spark plasma sintering [J]. Materials Science and Engineering B, 2002, 90(1−2): 34−37.

[27] KIM H, KAWAHARA M, TOKITA M. Specimen temperature and sinterability of Ni powder by spark plasma sintering [J]. Journal of the Japan Society of Powder and Powder Metallurgy, 2000, 47(8): 887−891.

[28] IVANOV V E, NECHIPORENKO E P, ZMII V I. Research diffusion in Mo−Si system [J]. Fizika Metallov i Metallovedenie, 1964, 17: 94−99.

[29] DARKEN L S, GURRY R W. Physical chemistry of metals [M]. New York: McGraw-Hill Inc., 1953.

[30] ZHANG Zhao-hui, WANG Fu-chi, LUO Jie, LEE Shu-kui, WANG Lu. Processing and characterization of fine-grained monolithic SiC ceramic synthesized by spark plasma sintering [J]. Materials Science and Engineering A, 2010, 527(7−8): 2099−2103.

放电等离子烧结制备 $SiC/MoSi_2$ 复合材料的显微组织、烧结行为及力学性能

韩欣欣，王雅雷，熊 翔，李 恒，陈招科，孙 威

中南大学 粉末冶金国家重点实验室，长沙 410083

摘 要：以 Mo、Si 和 SiC 粉末为原料，利用放电等离子烧结技术在不同温度下制备 $SiC/MoSi_2$ 复合材料，研究 $SiC/MoSi_2$ 复合材料的物相组成、显微组织和力学性能，并探讨其烧结行为。结果表明：$SiC/MoSi_2$ 复合材料由 $MoSi_2$、SiC 和少量的 $Mo_{4.8}Si_3C_{0.6}$ 组成，呈现细晶组织。在 $SiC/MoSi_2$ 复合材料的烧结过程中，存在固相烧结至液相烧结的演变。1600 °C 烧结的 $SiC/MoSi_2$ 复合材料表现出最好的力学性能，其维氏硬度、抗弯强度、断裂韧性分别为 13.4 GPa、674 MPa 和 5.1 $MPa·m^{1/2}$，比纯 $MoSi_2$ 分别提高了 44%、171%和 82%。第二相 SiC 作为硬质相可以承受外加应力，并阻碍裂纹的快速扩展，有助于复合材料力学性能的提高。

关键词：$SiC/MoSi_2$ 复合材料；显微组织；烧结行为；力学性能；放电等离子烧结

(Edited by Xiang-qun LI)